Journal of Fluids and Structures 27 (2011) 848–854

Contents lists available at ScienceDirect

Journal of Fluids and Structures

journal homepage: www.elsevier.com/locate/jfs

Flow around a tethered cylinder, the effect of tether length at high layover angles

Kris Ryan

Fluids Laboratory for Aeronautical and Industrial Research (FLAIR), Department of Mechanical and Aerospace Engineering, Monash University, Victoria 3800, Australia

ARTICLE INFO

Article history:
Received 24 October 2010
Received in revised form
23 February 2011
Accepted 10 March 2011
Available online 2 May 2011

Keywords:
Vortex-induced vibration
Tethered cylinder systems

ABSTRACT

Tethered cylinder systems constitute a natural extension of the lightly damped, hydro-elastically mounted cylinder. In this case, the cylinder is constrained to travel along an arc prescribed by the tether length. The analysis of the tethered cylinder system is hampered by the dependence of the natural frequency of the system on both the fluid forces acting on the system and the curved motion (which in turn alters the added mass coefficient away from unity). These difficulties have precluded prior studies considering the natural frequency or reduced velocity as a controlling parameter, making direct comparison with the hydro-elastically mounted cylinder system difficult.

This investigation considers the case of a tethered cylinder at low Reynolds number ($Re=200$) for a mass ratio $m^*=0.2$. It notes a local maximum in the amplitude of oscillation when the normalized tether length $L^* \simeq 2.0$, in agreement with prior studies. By instead considering the amplitude of oscillation in a rotational framework, we are able to explain the existence of this peak, and identify two regions of amplitude response, the first region exists for very small tether lengths ($L^* \lesssim 0.3$), while the second exists for larger tether lengths. The transition from small tether lengths to large tether lengths exhibits the highest amplitude angular oscillations.

Several wake states are also considered for a tethered cylinder which is oscillating about a horizontal mean layover angle. By considering these wake states, coupled with the definition of the natural frequency, an estimate of the added mass coefficient is made. Here we predict that $C_A \simeq 0.5$ for a tether length of $L^*=1.5$. This prediction is based not only on the tether length, but also on the amplitude of oscillation, and hence is Reynolds number dependent.

1. Introduction

Vortex-induced vibration of cylindrical structures remains as a key engineering challenge worldwide, with particular application in the oil, gas, and electrical transmission industries. The synchronization of the vortex shedding to the natural frequency of the oscillating structure (referred to commonly as 'lock-in') typically enhances the amplitude of oscillation, and may result in structural failure (see for example Sarpkaya, 2004).

Research into this phenomenon is generally classified into two broad categories based on the model under investigation. The first category has considered the flexibility of the oscillating cylinder as a key parameter—which may allow for the transmission of oscillation along the cylinder itself (see for example the work of Vandiver et al. (2009)). The second category

E-mail address: kris.ryan@monash.edu

0889-9746/$ - see front matter © 2011 Elsevier Ltd. All rights reserved.
doi:10.1016/j.jfluidstructs.2011.03.012

has instead considered the oscillation of a rigid cylinder. This second category, while simpler than the first, allows for an in-depth understanding of the direct relationship between the Strouhal shedding cycle and the cylinder oscillation (Williamson and Govardhan, 2004).

The tethered cylinder may be considered as an extension of the more familiar (and widely studied) freely oscillating rigid cylinder. In particular, assuming that the tether does not provide significant mechanical damping it directly extends the work of Govardhan and Williamson (2000, 2003). In particular, as with a lightly damped oscillating cylinder, the tethered cylinder system exhibits a critical mass ratio, below which large amplitude oscillations are observed for a wide range of inflow conditions (Ryan et al., 2007). This critical mass ratio is observed to vary as a function of tether length.

As a part of their work, Ryan et al. (2007) observed a peak in maximum oscillation amplitude (for the particular case of $m^* = 0.2$) at a tether length ratio of $L^* \simeq 2.0$. However, no explanation for this local maximum was presented therein.

Additionally, Ryan et al. (2007) noted that, unlike the freely oscillating cylinder, the equation for the natural frequency of the tethered cylinder was non-linear and may be directly related to the instantaneous fluid forces acting on the cylinder. For this reason a clear definition of the reduced velocity was impractical, and Ryan et al. (2007) introduced a modified Froude number to model the ratio of inertial to buoyancy forces.

This paper explores the reasons for the local peak observed at $L^* \simeq 2.0$ by Ryan et al. (2007), in addition to describing the structures in the wake of the cylinder as a function of tether length. By comparing these wake structures to those observed in the wake of a freely oscillating cylinder, it is possible to estimate the natural frequency of the system.

2. Model definition

Fig. 1 describes the geometry of the problem. A cylinder is attached to a massless, inflexible tether whose length may be described as the length ratio, $L^* = L/D$, where L is the length of the tether, and D is the diameter of the cylinder. An additional controlling parameter is the cylinder mass ratio, m^*, defined as the ratio of the density of the cylinder to that of the working fluid. The equation of motion for the system may be written as

$$J\ddot{\phi} + TL^*D\phi = F_{osc}L^*D, \tag{1}$$

where J is the moment of inertia of the tethered body system, T is the tension within the tether, F_{osc} describes the fluid force acting to oscillate the body (that is the component of fluid forces in the direction tangent to the tether direction) and ϕ describes the angular position of the cylinder about the mean layover angle θ. Details of the system may be found in Ryan (2004). In particular, the moment of inertia is defined exactly as

$$J = mD^2\left(L^{*^2} + \frac{1}{8}\right), \tag{2}$$

with m representing the mass of the cylinder per unit span.

3. Numerical techniques employed

The algorithm employed considers a two-dimensional domain such that effects of side-forces acting in the span-wise direction are neglected. In the present numerical study the restraining tether is assumed massless, in-elastic and is

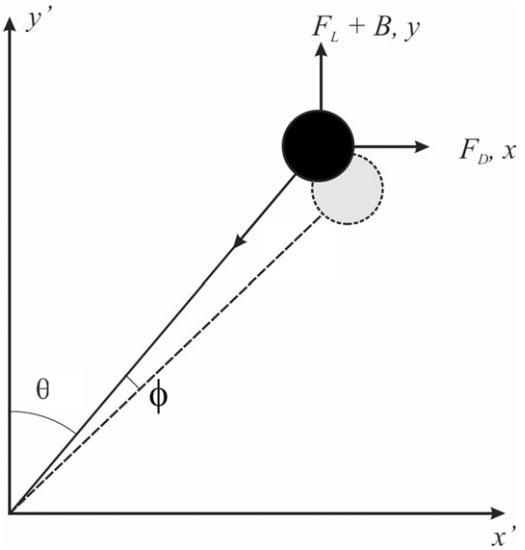

Fig. 1. Tethered cylinder geometry and coordinate system.

assumed to have a diameter significantly smaller than the cylinder, such that any fluid loading forces acting directly on the tether may be ignored. The cylinder is attached to the tether such that its motion remains attached to the arc defined by the tether radius (that is the cylinder does not "nod" about the point which it is attached to the cylinder). Wall and floor effects are neglected. This point is especially important as a nearby surface would invariably influence the fluid forces acting on the cylinder, and the response of the system in its entirety.

The numerical technique solves the two-dimensional form of the Navier–Stokes equations, expressed in primitive variable form:

$$\frac{\partial \mathbf{u}}{\partial t} + \mathbf{u} \cdot \nabla \mathbf{u} = -\nabla p + \nu \nabla^2 \mathbf{u} + \mathbf{A}, \tag{3}$$

$$\nabla \cdot \mathbf{u} = 0, \tag{4}$$

where p is the kinematic pressure, ν is the kinematic viscosity, $\mathbf{u} = (u(t,x,y), v(t,x,y))$ is the two-dimensional velocity vector, and $\mathbf{A}$ is an additional acceleration term due to the solution being conducted in an inertial reference frame. Spatial derivatives are evaluated using spectral-element discretizations as described by Karniadakis and Henderson (1998), and employed in similar studies by Ryan et al. (2004, 2005). Temporal derivatives are evaluated using a third-order time-splitting technique following the work of Karniadakis et al. (1991).

The Navier–Stokes equations are coupled with the kinematic equations describing the motion of the tethered cylinder, these equations may be written as:

$$m\ddot{x} = F_D - T\sin(\theta + \phi), \tag{5}$$

$$m\ddot{y} = (F_L + B) - T\cos(\theta + \phi), \tag{6}$$

where F_D is the measured drag force, F_L is the measured lift force, and B is the force due to buoyancy effects. Note that drag and lift forces are measured directly and consist of both viscous and pressure contributions. The motion of the cylinder is calculated within an inertial reference frame (with acceleration $\mathbf{A}$) attached to the cylinder. Having the reference frame of the computational grid attached to the cylinder greatly simplifies the problem, and allows for rigorous domain and resolution analysis studies to take place.

Eqs. (5) and (6) are coupled with the Navier–Stokes equations through a third-order Adams–Bashforth/Adams–Moulton method, described in detail in Ryan (2004). Each time step requires a series of sub-steps to be conducted such that the fluid velocity, and the forces acting on the cylinder reach satisfactory convergence prior to the calculation of the next time step.

4. Computational details

To agree with the prior work of Ryan et al. (2007), we restrict our attention to Re=200 (where the Reynolds number is based on the cylinder diameter and the inlet velocity, U). It was decided that this was the highest Reynolds number which could be considered using a two-dimensional domain. In addition, we consider only one mass ratio, $m^*=0.2$ and a wide range of tether length ratios, $L^*=[0.1, 10]$. Note that the tether length is measured from the center of the cylinder, such that for $L^*=0.5$, the cylinder is oscillating about a pivot point attached to its surface.

Following a domain analysis study, a mesh with an inlet 15 diameters upstream of the leading edge of the cylinder, and the outlet 23 diameters downstream of the trailing edge of the cylinder was chosen. Domain side-walls are 30 diameters apart. In all, the computational grid consisted of 518 macro-elements. Simulations conducted on larger domains had a less than 1% difference on peak fluid forces and shedding Strouhal number, measured across several cycles of saturated motion, when compared to the current mesh; indicating that the boundaries on the current domain do not interfere with the flow around the cylinder.

A rigorous p-type grid resolution study was conducted. Based on this investigation, ninth-order polynomials were used as interpolating polynomials within each macro-element. Peak fluid forces and Strouhal number measured about a fixed cylinder at Re=200 varied by less than 1% for $p=9$, when compared to higher order interpolation polynomials.

Typically, the controlling parameter considered for freely oscillating bodies is the reduced velocity $U^* = U/f_n D$, where f_n is the natural frequency of the system. However, the natural frequency cannot be determined *a-priori* for the tethered body system, as it is dependent on the tension acting through the tether, and hence on the fluid forces acting on the system, with the definition

$$f_n = \sqrt{\frac{T \cdot L^*}{(m + m_A) D \left(L^{*2} + \frac{1}{8} \right)}}. \tag{7}$$

Here, m_A is the added mass of the system. It is noted that the incorporation of the added mass implies that the natural frequency is defined for the system immersed within the working fluid. As noted by Newman (1977), the rotational motion of the cylinder precludes an analytical estimate of the added mass (unlike the case of the freely oscillating cylinder where we may assume that $m_A \simeq \rho_w \mathbb{V}$; where ρ_w is the density of the working fluid and $\mathbb{V}$ is the volume of the cylinder). Instead, we follow the work of Ryan et al. (2007) and Carberry and Sheridan (2007) by employing the reduced Froude number as

the controlling parameter, where

$$\mathrm{Fr}' = \frac{U}{\sqrt{(gD)(1-m^*)}}. \tag{8}$$

Here g is the acceleration due to gravity. The reduced Froude number may be defined as the ratio of inertial to buoyancy forces acting on the cylinder. High values of Fr' correspond to $\theta \to 90^\circ$.

5. Results and discussion

Ryan (2004) found that, for all cases, the peak amplitude of oscillation of the tethered cylinder occurred at high Froude numbers (that is where the inertial forces dominate the buoyancy forces). For this reason, a Froude number of $\mathrm{Fr}' = 50$ was considered in this investigation. At this value of Fr', the cylinder's mean layover angle is $\theta \simeq 90^\circ$. This choice of Fr' means that the system most closely resembles that of the freely oscillating cylinder considered by (for example) Govardhan and Williamson (2000, 2003). By considering this Froude number, the cylinder oscillates predominantly transverse to the free-stream, and the effect of induced curvature of motion may be considered directly.

Results at higher Froude numbers were not found to deviate significantly from those obtained at $\mathrm{Fr}' = 50$, while the peak forces, and amplitude of oscillation was found to decrease as the reduced Froude number decreased.

5.1. The effect of tether length on the peak amplitude of oscillation

Fig. 2(a) shows the peak amplitude of oscillation of the cylinder for $\mathrm{Fr}' = 50$ for all tether lengths considered. In this figure the amplitude is defined as the peak displacement of the cylinder away from its mean position normalized by the cylinder diameter. Here, we define $\hat{A}^*$ as the peak oscillation amplitude for a given simulation, normalized by the cylinder diameter. A peak in oscillation amplitude at $L^*=2.0$ is observed in agreement with the findings of Ryan et al. (2007). The oscillations at this tether length are noteworthy with amplitudes greater than $0.5D$, quite significant considering the relatively low Reynolds number considered. Fig. 2(b) again shows the variation of oscillation amplitude; however, this time defined as the angular amplitude of oscillation about the pivot point. The two definitions are related through

$$\hat{A}^* = L^* \sin(\hat{\phi}). \tag{9}$$

From Eq. (9), our observation in Fig. 2 that $\hat{\phi} \to 0$ as $L^* \to \infty$, and , $\hat{A}^* \to 0$ as $L^* \to 0$, is not surprising. However, we note two distinct trends in $\hat{\phi}$ as a function of L^*. For $L^* < 0.3$, a linear increase in $\hat{\phi}$ is noted; while for $L^* \geq 0.3$ a decay in $\hat{\phi}$ is noted.

For $L^* < 0.3$, the linear increase in $\hat{\phi}$ may be understood by assuming that the fluid forces acting on the cylinder do not alter appreciably across the range $L^*=[0,0.3]$. With this assumption, the amplitude of the moment acting to oscillate the body ($F_{osc}L^*D$) varies linearly with L^*. In addition, the moment of inertia of the system (Eq. (2)) does not change appreciably across this range; indeed for tether lengths below $L^{*2} \simeq 1/8$, the moment of inertia is virtually independent of any variation in tether length. Thus it is the linear increase in the amplitude of the moment acting on the body which results in the linear increase in oscillation amplitude. This assumes that the shedding frequency is far from the natural frequency of the system.

For $L^* > 0.3$ a decay in $\hat{\phi}$ is noted, which in general is found to found to fit

$$\hat{\phi} = \frac{a}{L^*}. \tag{10}$$

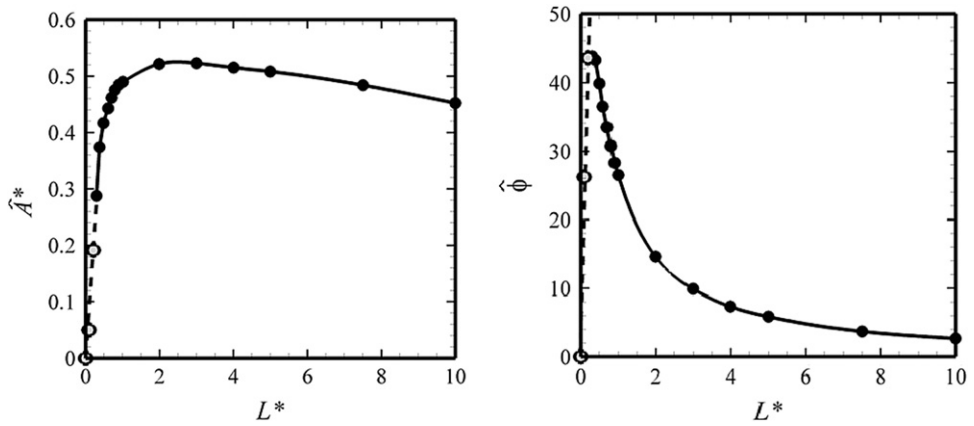

Fig. 2. Amplitude of oscillation results as a function of L^* for $m^*=0.2$ and $\mathrm{Fr}' = 50$— representing the highest amplitude response for all Fr' considered. Left hand side: response plot as the translation of the cylinder centre of mass. Right hand side: response plot as angular rotation (measured in degrees) of the cylinder centre of mass.

Here, the coefficient a is dependent on the cylinder mass ratio and Reynolds number. For our case, an excellent fit is observed when $a=28.12$.

The form of Eq. (10) may be derived through inspection of the equations of motion in a manner similar to that described by Govardhan and Williamson (2003). Here, we assume a sinuous oscillation (restricted to considering only one temporal frequency of oscillation), such that the equation of motion (Eq. (1)) may be rewritten as

$$-4\pi^2 f^2 J\hat{\phi} + \overline{T}L^* D\hat{\phi} = \hat{F}_{osc} L^* D\cos(\theta_{lag}). \tag{11}$$

Here, f is the temporal frequency of oscillation of the tethered cylinder system, $\hat{F}_{osc}$ is the peak oscillation force, and θ_{lag} is the phase angle between the force signal and the cylinders motion. In addition, Eq. (11) assumes that the tension in the tether throughout the oscillation cycle can be well approximated by the mean tension $\overline{T}$.

Eq. (11) may be rewritten such that $\hat{\phi}$ is the subject of the equation to form

$$\hat{\phi} = \frac{\hat{F}_{osc}\cos(\theta_{lag})}{\overline{T} - 4\pi^2 f^2 mD\left(L^* + \dfrac{1}{8L^*}\right)}. \tag{12}$$

For the fluid forces to drive the motion of the cylinder, $\cos(\theta_{lag}) < 0$. Assuming that $\hat{F}_{osc}\cos(\theta_{lag})$ does not vary appreciably for $L^* > 0.3$, and that $4\pi^2 f^2 mD(L^* + (1/8L^*)) \gg \overline{T}$ for $L^* > 0.3$ then the form of Eq. (12) reverts to that of Eq. (10). Small errors in the trend-line, when compared to measured data, can be attributed to the stated two assumptions that are essentially stating that the physics underpinning the fluid-structure interaction does not change appreciably for the fully laid over cylinder with $L^* > 0.3$. While this is the case for the current simulations (being conducted at a low Reynolds number), these assumptions may not hold for higher Reynolds number flows (with potentially large changes in the maximum force acting on the cylinder across a range of L^*).

The peak in $\hat{A}^*$ observed by Ryan (2004) is therefore due to the variation in $\hat{\phi}$, coupled with the definition of $\hat{A}^*$ (Eq. (9)). Considering the system in a rotational framework allows us to clearly elucidate why this increase in $\hat{A}^*$ occurs.

5.2. The effect of tether length on wake response

Snapshots of the vortex structures in the wake of the tethered cylinder are shown in Fig. 3 for all tether lengths considered. In each case $\mathrm{Fr}' = 50$ corresponding to $\theta \simeq 90^\circ$. This value was chosen such that the effect of varying L^* could be

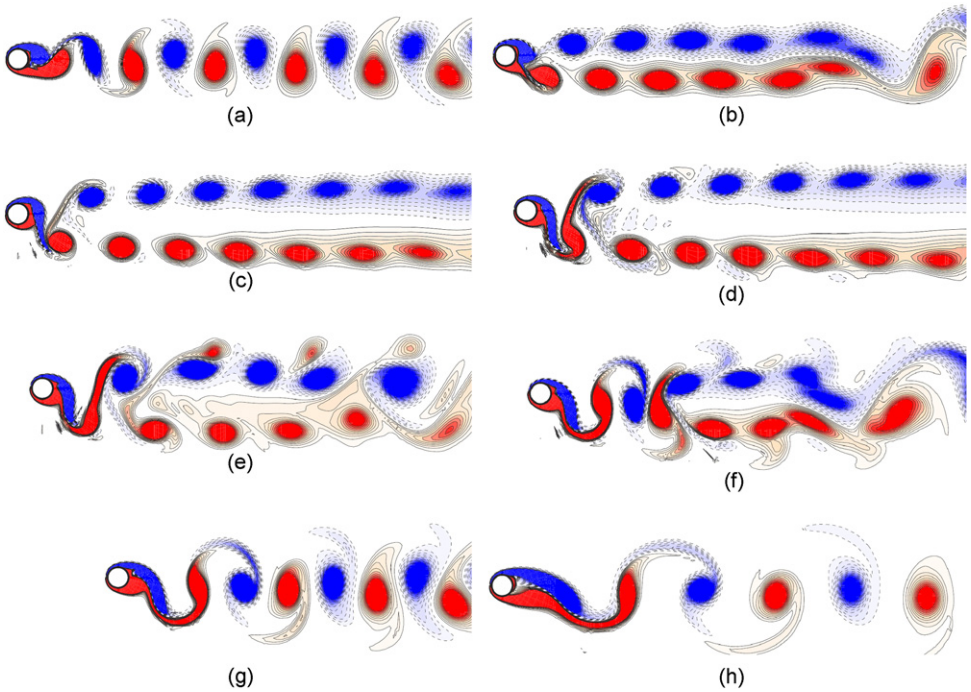

Fig. 3. Instantaneous snapshots of the span-wise vorticity field, ω_z, as a function of tether length. Contours are evenly spaced over the range (blue) $-1 \le \omega_z \le 1$ (red). All images are at the instant where the cylinder reaches the top of the oscillating cycle; (a) $L^*=0.1$, (b) $L^*=0.3$, (c) $L^*=0.5$, (d) $L^*=1.0$, (e) $L^*=1.5$, (f) $L^*=2.0$, (g) $L^*=5.0$, (h) $L^*=10.0$. (For interpretation of the references to color in this figure legend, the reader is referred to the web version of this article.)

observed without the complications induced by a finite mean lift coefficient and the accompanying vortex pairing in the wake and mean angle at which the wake is shed (see Ryan et al. (2007) for more details).

For $L^*=0.1$, the vortex structures are not dissimilar to the Kármán vortex street observed from a stationary cylinder, which is anticipated given the very low $\hat{A}^*$ observed. As L^* is increased to 0.3 (Fig. 3(b)), a significantly different wake is observed. Here $\hat{A}^* > 0.3$, and this has proved sufficient to alter the wake to form a double shear layer similar to that observed by Dusek et al. (1994) for a fixed cylinder. The double shear layer is observed to become unstable approximately 15 diameters downstream and forms a Kármán wake thereafter. This double shear layer wake is observed for the range $L^*=[0.3,1.0]$, corresponding to cylinder oscillation amplitudes less than $0.5D$. The width of the double shear layer increases with increasing tether length.

As the tether length is increased to $L^*=1.5$, the double shear layer wake is replaced with a "$P+S$" structure described experimentally by Williamson and Roshko (1988) and observed by Blackburn and Henderson (1999) for the case of an oscillating cylinder at low Reynolds number. In agreement with the current findings, Blackburn and Henderson (1999) report a very small mean positive lift for this wake structure. For $L^*=2.0$, the near-wake is similar to the Kármán vortex street, however, instabilities in the wake cause the formation of a double shear layer approximately seven diameters downstream of the cylinder prior to a further instability of the double shear layer further downstream. For $L^*=5.0$ and 10.0, the formation length is considerably longer and appears to increase with tether length.

5.3. Calculation of a natural frequency within the working fluid

The natural frequency of the system is dependent on the fluid forces acting on the cylinder, and cannot be predicted accurately *a-priori*. However, an estimate of the natural frequency can be made by assuming that the tension in the tether remains relatively constant throughout the oscillation cycle, and incorporating the measured lift and drag coefficients. Eq. (7) may be rewritten, such that the natural frequency of the system, immersed within the working fluid, may be explicitly calculated as

$$f_n = \frac{U}{D}\sqrt{\frac{2C_T}{\pi(m^*+C_A)L^*}}, \tag{13}$$

$$C_T = \frac{T}{\frac{1}{2}\rho_w U^2 D}, \tag{14}$$

where C_T is the tension coefficient per unit span of the cylinder, ρ_w is the density of the working fluid, and C_A is the added mass coefficient. When θ is large, the drag forces dominate the tension in the tether, and we may assume that $C_T \simeq C_D$, where C_D is the drag coefficient.

The key impediment to determining the natural frequency of the system in the working fluid is that the added mass coefficient cannot be assumed to be unity (as is the case for the freely oscillating cylinder) due to the curvature of the cylinder path. However, we may write that as $L^* \to \infty$, $C_A \to 1$, and as $L^* \to 0$, $C_A \to 0$. Hence, for sufficiently large tether lengths we can approximate $C_A \simeq 1$.

Fig. 4 shows the ratio of the oscillation frequency f with the natural frequency of the system, incorporating the added mass of the system, as a function of L^*. Throughout the range of tether lengths considered, a wide range of f/f_n is noted as a function of the assumed values of C_A considered. In particular, at $L^*=1.5$, the range of $f/f_n \simeq [0.8,1.6]$. This agrees closely with the range of values that Govardhan and Williamson (2000) predict that a freely oscillating cylinder will switch oscillation branches from the 'initial' branch to the 'upper' branch. Considering Fig. 3(e), we note that the $P+S$ shedding mode for the tethered cylinder, would be anticipated for a freely oscillating cylinder oscillating in the 'upper' branch at low Reynolds numbers. Analysis of Fig. 3(e) allows us to predict that $C_A < 1$ for $L^*=1.5$, this is not surprising given the high

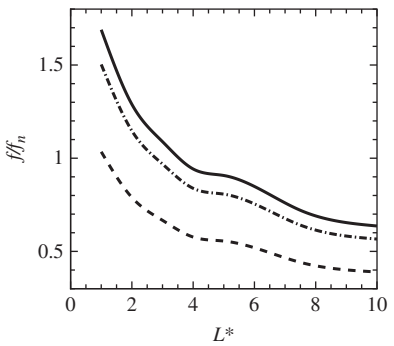

Fig. 4. Estimates of the frequency ratio f/f_n. Solid line, $C_A=1.0$; dash-dot line, $C_A=0.75$; dashed line, $C_A=0.25$.

value of $\hat{\phi}$ observed at this tether length. The author tentatively predicts that $C_A \simeq 0.5$ for this tether length and Reynolds number.

Thus direct comparison of the wake structures found for the tethered cylinder with that of the freely oscillating cylinder (at a similar Reynolds number) allows for a direct comparison of the mechanisms governing oscillation to be made. The strong similarity in the response of both systems makes this possible.

6. Conclusions

While the translational oscillation of a tethered cylinder is undoubtedly of great interest, the analysis of motion should be conducted in a rotational framework, as this provides a clearer description of the physics underpinning the cylinder motion. In addition, by carefully analyzing the wake states for various tether lengths, and comparing these to that obtained for a hydro-elastically mounted cylinder, a prediction of the added mass coefficient can be made for the tethered cylinder system. This analysis is restricted to the case of a tethered cylinder system oscillating about a horizontal mean layover angle, as the focus of prior hydro-elastically mounted cylinder studies have dominantly considered this case.

Acknowledgments

The author would like to thank professors M. Thompson and K. Hourigan for their valuable insight in discussions leading to the production of this manuscript.

This research was undertaken in part using the NCI (National Facility in Canberra, Australia), thanks to a Merit Allocation Scheme grant. NCI is supported by the Australian Commonwealth Government.

References

Blackburn, H., Henderson, R.D., 1999. A study of two-dimensional flow past an oscillating cylinder. Journal of Fluid Mechanics 385, 255–286.
Carberry, J.J., Sheridan, J., 2007. Wake states of a tethered cylinder. Journal of Fluid Mechanics 592, 1–21.
Dusek, J., Fraunie, P., Gal, P.L., 1994. Local analysis of the onset of instability in shear flows. Physics of Fluids 6, 172–186.
Govardhan, R.N., Williamson, C.H.K., 2000. Modes of vortex formation and frequency response of a freely vibrating cylinder. Journal of Fluid Mechanics 420, 85–130.
Govardhan, R.N., Williamson, C.H.K., 2003. Resonance forever: existence of a critical mass and an infinite regime of resonance in vortex-induced vibration. Journal of Fluid Mechanics 473, 147–166.
Karniadakis, G.E., Henderson, R.D., 1998. Spectral element methods for incompressible flows, The Handbook of Fluid Dynamics. CRC Press (pp. 29-1–29-41.).
Karniadakis, G.E., Israeli, M., Orszag, S., 1991. High-order splitting methods of the incompressible Navier–Stokes equations. Journal of Computational Physics 97, 414–443.
Newman, J., 1977. Marine Hydrodynamics, first ed. MIT Press.
Ryan, K., 2004. The analysis of wake structures behind stationary, freely oscillating and tethered cylinders. Ph.D. Thesis, Monash University, Monash.
Ryan, K., Pregnalato, C., Thompson, M.C., Hourigan, K., 2004. Flow-induced vibrations of a tethered cylinder. Journal of Fluids and Structures 19, 1085–1102.
Ryan, K., Thompson, M.C., Hourigan, K., 2005. Variation in the critical mass ratio of a freely oscillating cylinder as a function of Reynolds number. Physics of Fluids 17, 038106.
Ryan, K., Thompson, M.C., Hourigan, K., 2007. The effect of mass ratio and tether length on the flow around a tethered cylinder. Journal of Fluid Mechanics 591, 117–144.
Sarpkaya, T., 2004. A critical review of the intrinsic nature of vortex-induced vibrations. Journal of Fluids and Structures 19, 389–447.
Vandiver, J.K., Jaiswal, V., Jhingran, V., 2009. Insights on vortex-induced, traveling waves on long risers. Journal of Fluids and Structures 25, 641–653.
Williamson, C.H.K., Govardhan, R., 2004. Vortex induced vibration. Annual Review of Fluid Mechanics 36, 413–455.
Williamson, C.H.K., Roshko, A., 1988. Vortex formation in the wake of an oscillating cylinder. Journal of Fluids and Structures 2, 355–381.